CO_2 Foam Behavior in Carbonate Rock
Effect of Surfactant Type and Concentration

Jones, Siân A.; Kahrobaei, Siavash; Van Wageningen, Niels; Farajzadeh, Rouhi

DOI
10.1021/acs.iecr.2c01186

Publication date
2022

Document Version
Final published version

Published in
Industrial and Engineering Chemistry Research

I&EC research
Industrial & Engineering Chemistry Research

pubs.acs.org/IECR

Article

CO_2 Foam Behavior in Carbonate Rock: Effect of Surfactant Type and Concentration

Siân A. Jones,* Siavash Kahrobaei, Niels van Wageningen, and Rouhi Farajzadeh

Cite This: *Ind. Eng. Chem. Res.* 2022, 61, 11977−11987

Read Online

ACCESS | Metrics & More | Article Recommendations | Supporting Information

ABSTRACT: An understanding of how CO_2 foam flows through a reservoir rock is useful for many subsurface applications, including enhanced oil recovery and CO_2 storage. There are economic and environmental benefits in identifying surfactants that exhibit good foaming behavior with CO_2 at both low concentrations and high foam qualities. Core flood experiments have been carried out to investigate the behavior of supercritical CO_2 foams flowing through a high-permeability Indiana Limestone. The foaming behavior and concentration response of two surfactants, a betaine and a sultaine, were investigated. For the two surfactants, the transition foam quality and the maximum apparent foam viscosity both decreased with reducing surfactant concentration. A comparison between the foaming behaviors of these surfactants with CO_2 and N_2 was also carried out. It was found that the N_2 generated stronger foam at low foam qualities, but the CO_2 was better at maintaining good foaming behavior at high foam qualities.

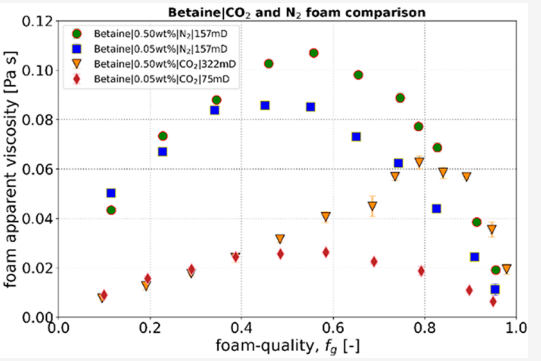

INTRODUCTION

An understanding of CO_2 flow behavior in rock is important for two reasons. First, the injection of CO_2 into an oil reservoir is a well-known and long-standing technique for improving oil recovery.[1−4] Second, carbon capture and storage (CCS), where CO_2 is captured and stored in existing reservoirs in order to reduce the quantity emitted into the atmosphere, is an important tool in combating the problem of global warming.[5−7]

Whether for enhanced oil recovery (EOR) or CCS, or a combination of the two,[8−12] the flow behavior of the CO_2 depends on both the microscopic sweep efficiency of the gas through the local rock structure and the macroscopic sweep efficiency. This latter is determined by the mobility ratio between the displacing fluid (injected gas) and displaced reservoir fluid. CO_2 generally provides excellent microscopic sweep, but for many reservoirs, it can be challenging to achieve an efficient macroscopic sweep, with thief zones, viscous fingering, and gravity override all affecting the stability of the displacement front. Generating a foam with the CO_2 is a well-known technique for viscosifying the gas, reducing any instabilities in the displacement front and enhancing sweep efficiency across the volume of the reservoir.[13,14] The foam can also assist in keeping the gas/liquid ratio low at the production well.

One of the major obstacles to the practical application of any foam is the cost of the surfactant. Working with a surfactant that exhibits good foaming behavior at both low concentrations and high foam qualities therefore gives strong economic and environmental benefits. Previous studies on the effect of surfactant concentration have been carried out using nitrogen gas in sandstone rocks.[15,16] However, very little, if any, work has been carried out on the effect of surfactant concentration on supercritical CO_2 foam, and the current study aimed to determine if the changing behavior with concentration is a general behavior, irrespective of gas or rock type, or whether changing the conditions will significantly change the concentration response.

It is also important to note that a large fraction, more than half, of the world's oil reservoirs are in carbonate formations.[17,18] The current work with CO_2 foam was therefore influenced by the importance of gaining a good understanding of CO_2 foaming behavior in carbonate rocks. Carbonates have different mineralogy, different surface chemistry,[19] and different morphology from sandstones. They can therefore produce different foaming behavior: for example, they may exhibit different or reduced foam generation mechanisms.[20,21] When choosing the type of surfactant to generate the foam, it is well-known that anionic surfactants exhibit high adsorptions in carbonates due to the attraction between the negatively charged surfactant and the positively charged carbonate rock surface.[22] Positively charged

Received: April 7, 2022
Revised: July 25, 2022
Accepted: July 26, 2022
Published: August 4, 2022

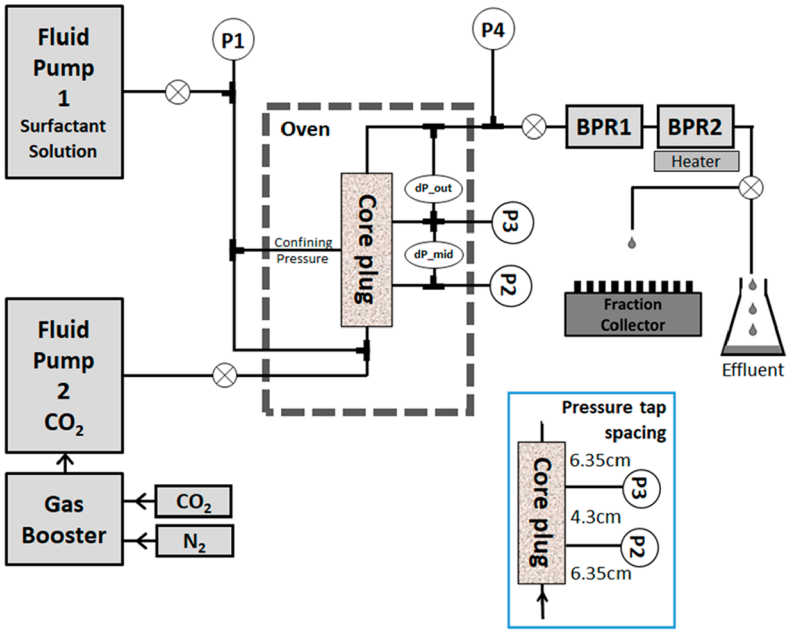

Figure 1. Schematic diagram of the core-flood setup that was used for both the dynamic adsorption and foam-flood tests. The pressure profile along the core was measured using both the four absolute pressure gauges (P1−P4) and the two differential pressure gauges (dP_mid and dP_out).

cationic surfactants exhibit lower adsorption on carbonate,[23] but these surfactants are typically costly and may not exhibit strong foaming behavior.[24] They also tend to exhibit high toxicity for aquatic organisms,[25] so they are not recommended for use in the subsurface. The recommendation is therefore to use nonionic or amphoteric surfactants with carbonate rocks.[26,27]

The current core floods were carried out in the highest permeability cores available, to reflect the fact that some reservoirs contain medium to high permeable carbonates due to diagenesis. Previous work has tended to focus on low-permeability chalks or fractured limestones,[28−31] and it is only recently that researchers have considered slightly higher permeability carbonate cores.[23,32] We therefore present here the results of a series of core floods carried out in Indiana Limestone cores with a wide range of permeabilities, from 75−673 mD. These core floods were used to determine the dynamic adsorption of two candidate amphoteric surfactants, their foamability in the carbonate rock, and the change in their behavior with changing surfactant concentration and gas type.

MATERIALS

Surfactants and Brines. Two amphoteric surfactants with good stability at the selected salinity were considered for testing: a sultaine (cocamidopropyl hydroxysultaine, AMPHOSOL CS-50, 48.6% activity) and a betaine (cocamidopropyl betaine, SURFAC B4, 30.5% activity). Both surfactants have the same C12 chain length. A four-salt synthetic seawater (TDS = 31.09 g/L, including 0.312 g/L of divalent ions) was used for all the stability and core flood tests. Solutions also included an oxygen scavenger, either 100 ppm of sodium sulphite (Na_2SO_3) or 100 ppm of carbohydrazide ($OC(N_2H_3)_2$), to minimize any oxidation issues during testing at elevated temperatures.

Rock Samples. A high-permeability Indiana Limestone, with core plugs of a diameter of 4 cm and length of 17 cm, was used for all the experiments. Due to the intrinsic heterogeneity of the block of high-permeability Indiana Limestone, the permeabilities of the core plugs varied a great deal, dependent on the exact location from which they were drilled. Core plugs with measured permeabilities (to water) in the range of 75−673 mD were obtained and used in the tests presented here. The porosity of the rock was measured using a pycnometer and was found to be 0.219 ± 0.005 (n = 6).

The Indiana Limestone cores were sealed with an epoxy resin (Rencast CW 47) and then mounted in a PEEK coreholder, before being connected into the core flood setup.

EXPERIMENTAL PROCEDURES

Surface Tension Measurements. The surface tensions of the two surfactants in the synthetic seawater were measured using a Kibron EZ-Pi tensiometer.[33] Initial solutions of 0.5 and 0.1 wt % surfactant in the seawater were made, and lower concentrations were generated by dilution with seawater. The surface tension was then plotted as a function of the log of the concentration, which allowed for the determination of the critical micelle concentration (CMC) for each surfactant.

Thermal Stability of Surfactants. The thermal stability of the surfactants was tested at 60 °C. Solutions with 1 wt % of surfactant in the synthetic seawater were made for both surfactants, along with 100 ppm of sodium sulphite as an oxygen scavenger. Approximately 200 mL volumes of the solutions were placed in 250 mL Duran bottles and then placed in an oven at 60 °C. Samples were removed from the oven at regular intervals to check for any signs of degradation or precipitation.

Dynamic Adsorption. The dynamic adsorption tests were carried out at 55 °C, using the core-flood setup (Figure 1) that was also used for the CO_2 foam tests. The Indiana Limestone cores, mounted in the PEEK coreholder, were placed in the oven and then fully saturated with synthetic seawater. The pressure in the core was set at 120 bar using the back-pressure regulators (BPR1 and BPR2). The permeability of the core was

https://doi.org/10.1021/acs.iecr.2c01186
Ind. Eng. Chem. Res. 2022, 61, 11977−11987

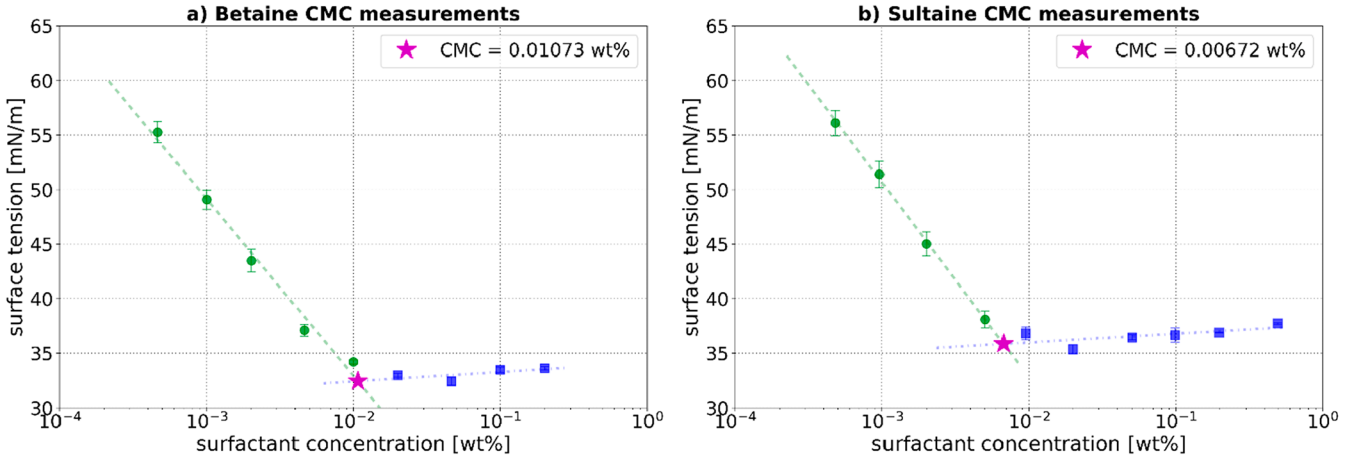

Figure 2. Surface tension plotted as a function of log(concentration) for (a) betaine and (b) sultaine.

measured with the synthetic seawater, before the adsorption measurement started.

Adsorption tests were carried out with 0.5 wt % of each surfactant in the synthetic seawater. Potassium iodide (KI) was used as the tracer, and 0.4 wt % was added to each surfactant solution. The oxygen scavenger used for all the core flood tests was 100 ppm of carbohydrazide, as there are known issues (possible gypsum formation) when using the sodium sulphite in a carbonate core.[27]

Between five and seven pore volumes of the solution were injected at 1 mL/min (equivalent to 1.47×10^{-5} m/s or 4.2 feet/day). The effluent was captured in the fraction collector with a sample size of 4 mL (~0.1 PV) each. The collected samples were than analyzed for (a) the KI concentration, by measuring the adsorption at 226 nm in a spectrophotometer, and (b) the surfactant concentration, approximated from the measured total organic content (TOC), which was determined using a Hach LCK381 spectrophotometer cuvette test. The concentrations of the KI and surfactant were then normalized for each sample, and these normalized values were plotted against the volume of solution injected. The difference in the transit time between the KI and the surfactant was then used to calculate the adsorption, either by considering the area between the two curves (which gives the total delayed volume) or by measuring the difference in the curves at the normalized concentration of 0.5 (when breakthrough occurs).[34]

Core Flood Tests − CO_2 Foam. The supercritical CO_2 foam tests were carried out using the apparatus shown in Figure 1, at a temperature of 55 °C, and with a back-pressure of 120 bar. This temperature was selected as being within the range of a known reservoir. The pressure was then fixed at 120 bar to ensure that the CO_2 was supercritical and that it would miscible with a model oil (decane) in future tests. Two back-pressure regulators were used to allow for a stepped drop in pressure at the outlet, when CO_2 was present in the system, to mitigate the side-effects associated with a sudden expansion of supercritical CO_2. A heater was also used to reduce the possibility of the effluent pipes freezing due to the expansion of the CO_2 (Joule−Thomson effect).

If a dynamic adsorption test had previously been carried out, the same Indiana Limestone core plug was left in place for the foam-flood. If a new, dry core was being used, it was first fully saturated with synthetic seawater. The permeability of the core at 90 °C was then determined, by measuring the pressure drop along the core, before saturating it with surfactant solution and flushing it for several pore volumes in order to satisfy the adsorption of surfactant on the rock.

Solutions of the two surfactants were made with the synthetic seawater and 100 ppm carbohydrazide. The surfactant solution was then coinjected with the CO_2 to give a total flow rate of 1.63 mL/min (equivalent to 2.4×10^{-5} m/s or 6.8 feet/day). To give the correct total flow rate and foam quality in the core, corrections had to be made to the CO_2 flow rate to take into account: (1) the volume of the gas lost due to solubility in the coinjected synthetic seawater (from the data of Duan et al.[35]) and (2) the difference in the CO_2 density between the room temperature pump and the core plug at 55 °C (using the equation of state from Span and Wagner[36]). A full description of these corrections can be found in refs 37 and 38 and the Supporting Information.

A range of foam qualities (f_g) were injected, where $f_g = u_g/(u_g + u_l)$, and u_g and u_l are the CO_2 and liquid superficial velocities, respectively. For every test, the initial injection was carried out at $f_g = 0.5$. This was followed by alternating low- and high-quality injections to avoid any hysteresis in the results.[16] The resultant steady-state pressure drop in the core (measured at dP_out) was used to calculate the apparent viscosity, μ_{app}, of the foam using Darcy's law

$$\mu_{app} = \frac{k\nabla P}{u_t}$$

where k is the rock permeability at the outlet of the core, calculated from dP_out before the start of the test, u_t (= u_g + u_l) is the total superficial velocity and ∇P is the pressure gradient measured at dP_out. Usually, the pressure gradient at the center of the core, calculated from dP_mid, is used when determining foam apparent viscosities. However, in this case, the pressure gradient at the outlet of the core, calculated from dP_out, was used, due to the technical challenges described in the Results (Technical Challenges) section.

The initial tests were carried out with 0.5 wt % surfactant concentration in each case, to give a baseline for the CO_2 foaming behavior in the Indiana Limestone. The behavior of the CO_2 foam with changing surfactant concentration was also investigated for both surfactants, with concentrations down to 0.01 wt % being tested.

Core Flood Tests − Nitrogen Foam. Nitrogen foam tests were also carried out to give additional information on the

https://doi.org/10.1021/acs.iecr.2c01186
Ind. Eng. Chem. Res. 2022, 61, 11977−11987

foam behavior with changing surfactant concentration. Nitrogen is useful as there are less technical challenges in carrying out multiple repeat tests with nitrogen than are observed with CO_2 (as discussed in the Results − Technical Challenges). There is therefore a greater degree of repeatability, over a larger number of tests, with the nitrogen foam.

To carry out the nitrogen tests, the setup in Figure 1 was again used, with the CO_2 fluid pump replaced by a nitrogen cylinder and mass flow controller. The core plug used for all the tests was an Indiana Limestone core with a permeability of 157 mD (measured at dP_out). When switching between the betaine and sultaine, the core was cleaned using an injection of 10 PV of a 50:50 solution of isopropyl alcohol in tap water to remove any residual surfactant from the core. The IPA mixture was then flushed with 10 PV of the synthetic seawater and 5 PV of the new surfactant solution, to satisfy the adsorption, before any new foam tests were carried out.

All foam experiments were carried out with a back-pressure of 40 bar and at a temperature of 65 °C. Solutions with a range of surfactant concentrations, from 0.5 down to 0.01 wt % in the synthetic seawater, were tested. The surfactant solution was coinjected with the nitrogen at the base of the core at a constant total flow rate of 1.63 mL/min, equivalent to a total superficial velocity, u_t, of 2.4×10^{-5} ms^{-1} (equivalent to 6.8 feet/day). A range of foam qualities (f_g) were injected, and dP_out was again used to calculate the apparent viscosity, μ_{app}, of the foams.

RESULTS AND DISCUSSION

Surface Tension Measurements. The surface tension of each surfactant, in solution with the synthetic seawater (TDS = 31.09 g/L) was measured at room temperature, with the aim of determining the CMC. A range of concentrations were considered, from 0.5 down to 0.0005 wt %. In each case, the surface tension was plotted against the log of the concentration (Figure 2), and the CMC was determined from the intersection of the decreasing and horizontal sections of the curve. The CMC for each surfactant is indicated on the respective graph.

Knowing the CMC for each surfactant assists in planning the core flood tests, as it suggests the lower limit of the range of concentrations that should be tested. Describing the surfactant concentration as a multiple of the CMC concentration also makes it easier to compare surfactants with greatly differing CMCs.

Thermal Stability of Surfactants. A thermal stability test was carried out with both the betaine and sultaine, using 2 wt % solutions in the synthetic seawater and with sodium sulphite as the oxygen scavenger. Both solutions showed good stability, with no cloudiness or precipitate, up to the 18 week duration of the tests (Figure 3).

It should be noted that an initial stability test was carried out with carbohydrazide as the oxygen scavenger. However, it was found that these initial samples with carbohydrazide developed a slight pink coloration after prolonged heating (>2 weeks). The reaction causing this is not known, or whether it has the potential to affect the surfactant stability, so the long-term (18 week) stability test was carried out with sodium sulphite as the oxygen scavenger.

Dynamic Adsorption. Dynamic adsorption tests were carried out for both of the surfactants, with 0.5 wt % solutions at 55 °C. Typical adsorption curves for each surfactant are given in Figure 4, showing the difference in the arrival time of the KI and each surfactant (from the TOC), at the exit of the core.

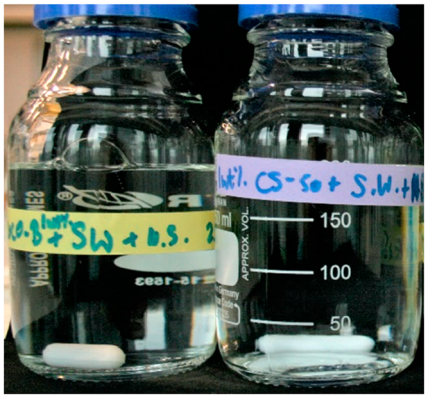

Figure 3. Image of the betaine (left-hand bottle) and sultaine (right-hand bottle) samples after aging in the oven at 60 °C for 18 weeks. The samples remained clear, with no precipitation or cloudiness.

Considering these adsorption curves, the value of the dynamic adsorption could be determined in two ways. Either the difference in arrival time between the two curves at a normalized concentration of 0.5 (black dashed lines) could be measured, or the area between the two concentration curves (orange shading on Figure 4a) could be determined. In both cases, the measurements allowed for the mass of retained surfactant to be calculated and thus the adsorption per 100 g of rock. The measured values are summarized in Table 1.

It was found that the sultaine and betaine had similar, relatively low values of retention. These values were in general agreement with previous obtained values: 12 mg/100 g of rock, for a betaine on Indiana Limestone at 23 °C;[39] 12.5−20.3 mg/100 g of rock, for a betaine-type amphoteric on natural carbonate at 100 °C;[40] and 25.7 mg/100 g of rock, for a betaine onto carbonate rock.[32]

It should be noted however that the concentration curves obtained for the surfactants are more asymmetrical than would usually be expected, with a long tail in the normalized surfactant concentration being seen in both cases. This long tail and asymmetric curve then resulted in the differences in adsorption values obtained for the two different measurement techniques. It is suggested that this asymmetry in the curves and the long tail is caused by a secondary retention mechanism, namely the mechanical entrapment of the surfactant micelles. This mechanical entrapment is more commonly seen in polymer core floods[41] and is not normally significant for surfactants, where the micelles are usually small in comparison to the pore sizes. However, the Indiana limestone has a complicated morphology, with a wide range of pore sizes, and regions of microporosity,[42] that make physical entrapment of micelles more likely. The complicated morphology may also mean that there are inaccessible pore volume effects.[43] It is therefore suggested that the value calculated using the area method may overestimate the adsorption, as it likely includes both adsorption and mechanical entrapment effects.

Core Flood Tests − CO_2 Foam. Foam-floods were carried out at 55 °C, with 0.5 wt % of the surfactants in synthetic seawater. All pressures for the apparent viscosity calculations were measured at the outlet of the core (dP_out) rather than in the midsection (dP_mid). The decision to work with dP_out was made after the first core flood test, where the

https://doi.org/10.1021/acs.iecr.2c01186
Ind. Eng. Chem. Res. 2022, 61, 11977−11987

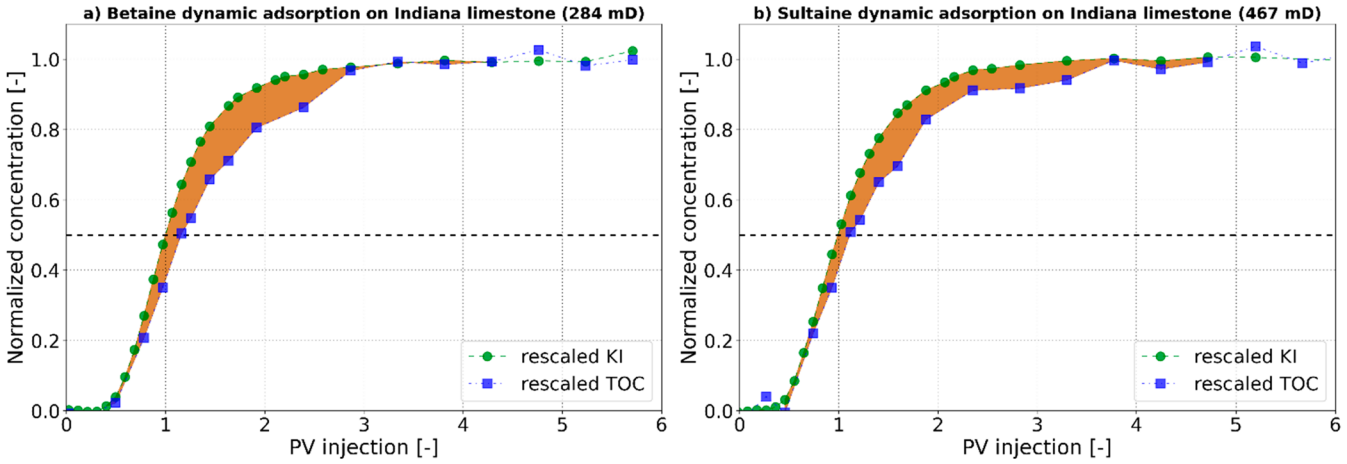

Figure 4. Normalized concentration curves for dynamic adsorption measurements, for (a) betaine and (b) sultaine. The average permeability of the limestone core for each test is indicated.

Table 1. Dynamic Retention Values for the Betaine and Sultaine

Surfactant	Dynamic adsorption, mg/100 g of rock (difference in curves at 0.5 concentration method)	Dynamic adsorption, mg/100 g of rock (area method)
Betaine	8.0	12.6
Sultaine	6.1	13.0

generation of wormholes within the rock due to CO_2 acid dissolution was found to occur very rapidly in terms of the time scale of the test. In each test, the degradation of the rock begins at the inlet surface, with the wormhole then propagating along the core. The pressure drop measurements at the entrance of the core are then reduced due to the local increase in permeability caused by the wormhole, and the foam generation zone is pushed further into the core, away from the inlet. So, the pressure drop at dP_mid can be affected by the wormhole, even before the wormhole propagates to the center of the core, and hence, the most reliable pressure measurements were obtained at dP_out (see the full discussion of this issue in the Technical Challenges section).

The variation in the pressure gradient at dP_out with the total pore volumes injected, for the tests with 0.5 wt % sultaine, is shown in Figure 5. The apparent viscosity curves for both surfactants are shown in Figure 6. It can be seen that both the sultaine and betaine have a good foaming response, with reasonably high values of apparent viscosity, and a transition foam quality of about 0.8 in both cases. It can be seen that the shape of the curve is not smooth around the transition for the sultaine. This is caused by the uncertainty in two of the data points, at f_g = 0.75 and 0.85. These were the last two tests carried out (see Figure 5), and it can be assumed that there was a high degree of core degradation by this time, so the measured viscosities were lower than expected.

Effect of Surfactant Concentration. CO_2 foam tests were also carried out with varying values of surfactant concentration (Figure 7). For both betaine and sultaine, changing the concentration did not affect the foam viscosity in the low-foam-quality regime, but there was the expected reduction in both the transition foam quality, f_g*, and the maximum apparent viscosity, μ_{max}, as the concentration decreased (as previously observed by Kahrobaei and Farajzadeh[16] and Jones et al.[15]). However, even with these

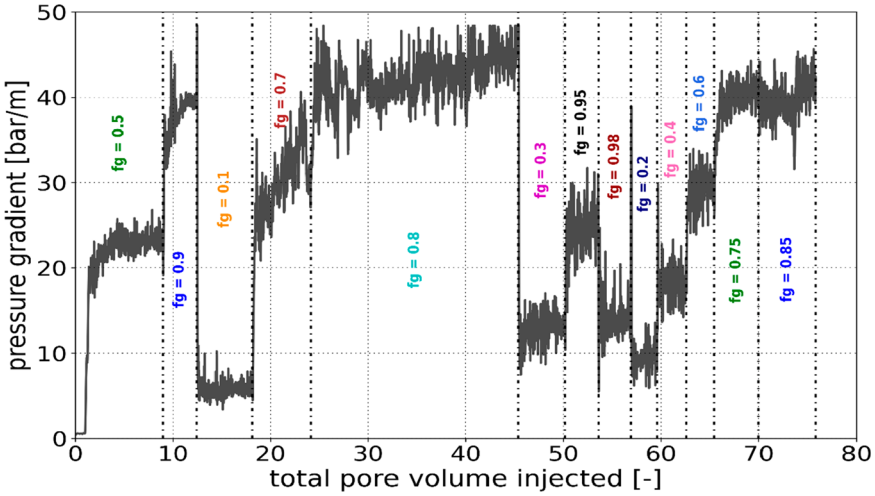

Figure 5. Variation in the pressure gradient at dP_out with the total pore volumes injected for the CO_2 foam-flood tests with 0.5 wt % sultaine.

https://doi.org/10.1021/acs.iecr.2c01186
Ind. Eng. Chem. Res. 2022, 61, 11977−11987

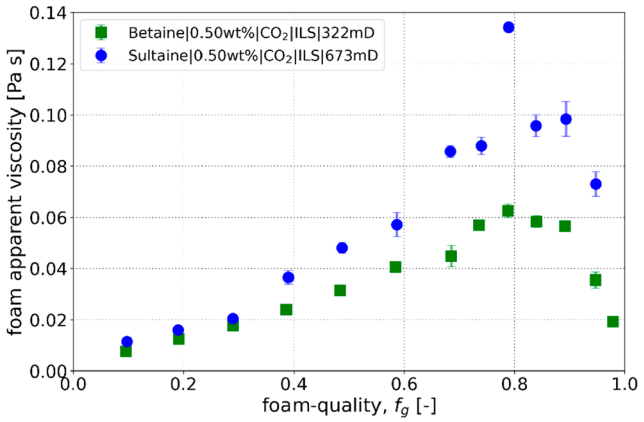

Figure 6. Foam quality scans for the two surfactants tested. The permeability (at dP_out) of the limestone core is indicated for each test.

expected changes, for both of these surfactants, and the betaine in particular, there was still reasonable foaming behavior at close to the CMC.

It is expected that higher permeability cores give higher measured apparent viscosities over the whole range of foam qualities. Brame et al.[44] discuss the relationship between the permeability and the shear rate experienced by the flow in a rock, with the shear rate scaling with $k^{-1/2}$. Foams in higher permeability rocks therefore experience lower shear rates and less shear thinning and hence give higher measured viscosities. This effect has been observed in previous tests in sand-packs,[44] sandstone cores,[45] and carbonate cores.[26] Unexpectedly, then, in this case, the foam scans for both the betaine and the sultaine (Figure 7) showed no effect of varying core permeability, with the curves lying together in the low-quality regime. However, as Brame et al.[44] also discuss, the heterogeneity of the rock can have an effect on the foaming behavior, with a higher degree of heterogeneity reducing the effect of the different bulk permeabilities.

Carbonates are known to be highly heterogeneous over a wide range of length scales,[46] with regions of macroporosity and microporosity,[42] as demonstrated in the micro-CT image of one of our Indiana Limestone cores (Figure 8). It can be seen that our sample contains grains with a wide range of sizes

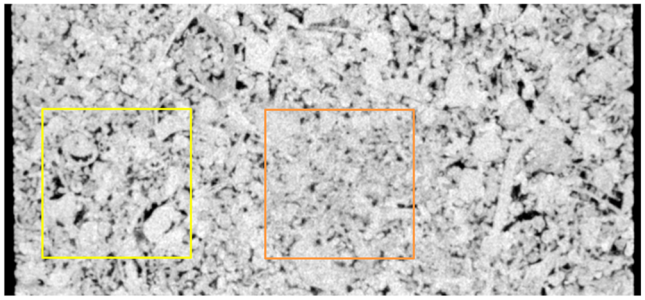

Figure 8. Micro-CT image of one of the Indiana Limestone cores used in the current tests. Longitudinal slice with a width of 4 cm and length of 1.8 cm. The colored boxes are 1 cm square and indicate zones of locally high (yellow) and locally low (orange) porosity.

and aspect ratios as well as regions of more dense or more open packing. This results in large variations in local porosity and permeability, across length scales of ~1 cm. It is suggested that this complexity in the rock structure, at the microscopic level, will decouple the foam behavior from the bulk (average) permeability of the core, as any foam moving through the core will interact with many regions of different local permeability.

Technical Challenges When Carrying out CO_2 Foam Tests in Carbonate Rock. It became obvious early in the program of experiments that there was a significant technical challenge associated with the injection of CO_2 into a limestone core, with the formation of wormholes within the rock due to acid dissolution.

The carbon dioxide reacts with water to form carbonic acid:

$$CO_2 + H_2O = H_2CO_3$$

And the carbonic acid then reacts with the carbonate rock to form a soluble salt:

$$CaCO_3 + H_2CO_3 \leftrightarrow Ca(HCO_3)_2$$

This soluble salt, in this case, calcium bicarbonate, is then carried out of the core with the effluent flow, gradually causing erosion of the rock. Degradation of the rock usually begins on the inlet surface, where several small holes can form (Figure 9b). Eventually, one of these small holes will become slightly more dominant, and this then becomes the main flow path into the rock. The erosion will then continue mainly along this

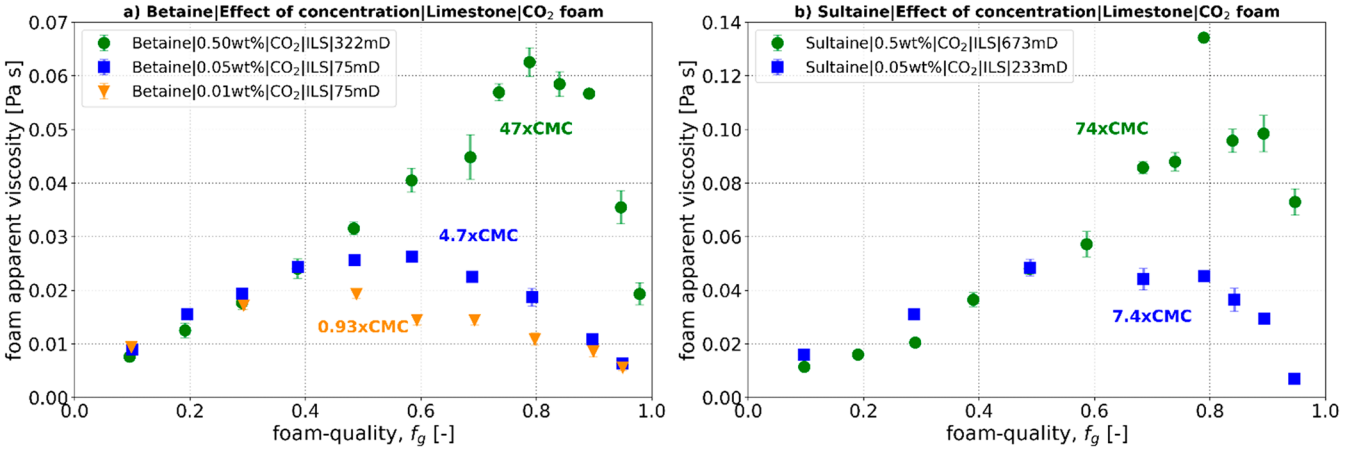

Figure 7. Variation in foam apparent viscosity with variation in surfactant concentration, for (a) betaine and (b) sultaine. The permeability of the limestone core for each test is indicated in the key, and the curves are also labeled with the concentrations in terms of the CMC.

https://doi.org/10.1021/acs.iecr.2c01186
Ind. Eng. Chem. Res. 2022, 61, 11977−11987

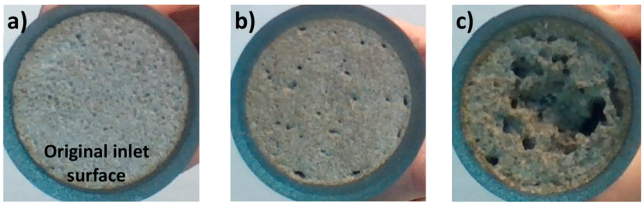

Figure 9. Images of the limestone core, showing (a) the original, undamaged inlet of the core, (b) early stage wormhole formation, and (c) major wormhole damage after extended testing.

preferential path, and a growing wormhole is formed (Figures 9c and 10).

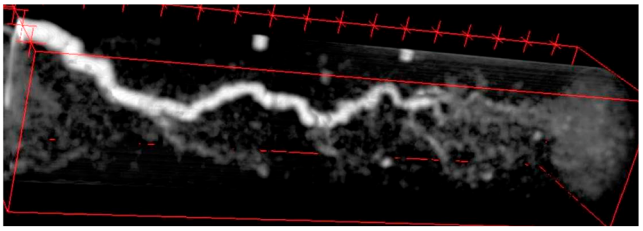

Figure 10. Image of a wormhole generated during a CO_2 foam flood. The injection was from the left side. The image is reconstructed from a CT-scan of the core, and void spaces are shown in white. The two white spots on the upper surface of the core are the points where the pressure taps were drilled.

These wormholes are significant in terms of the end use in EOR or CCS[47] where they can either beneficially improve the injectivity near the well or cause detrimental damage to the formation and the well/completion. However, of more immediate importance during the current foam-flood tests was the speed with which these wormholes could form, within a day from the start of injection in the worst cases, i.e., with only 50−60 PV injected. The speed of wormhole formation was probably dependent on the local structural variations in grain size, shape, and packing. Once the wormhole had been formed, it significantly altered the pressure measurements, due to the increase in permeability along the path of the wormholes, especially at the entrance of the core where there was most damage. Similar problems have also been described by Gland et al.[23] and Jian et al.[27]

It was observed that the most significant damage (as observed from the pressure traces) often occurred during the transition from one foam quality to another, i.e., when switching from a high CO_2 fraction to a high water fraction or vice versa. The reason for this is not known. For instance, a typical pressure trace observed at the inlet during wormhole formation is shown in Figure 11. The injected foam quality was altered from f_g = 0.7 to f_g = 0.3 at Time = 0, and it took just over half an hour for the pressure drop across the inlet to decrease from 1.4 bar to zero. After this time, nearly all the flow in the inlet section of the core was through the wormhole.

There are several experimental implications associated with this degradation of the core. Perhaps of most importance, the formation of a wormhole can result in uncertainties in the measured viscosities, which can in turn mean that only small data sets are obtained. When the rock structure at the inlet is compromised by the wormhole, this means that the foam generation zone is pushed further into the core, away from the inlet. This effect can be clearly seen in the apparent viscosities

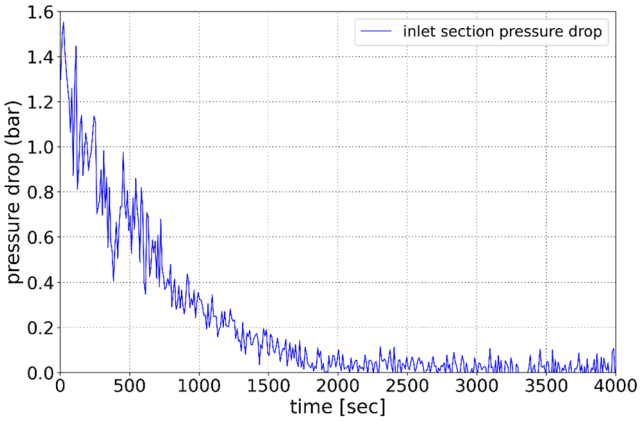

Figure 11. Pressure drop at the inlet of the core during significant wormhole formation. The foam quality had changed from f_g = 0.7 to f_g = 0.3 at the start of this test.

calculated from the middle-section pressure drop (dP_mid), where a significant drop in μ_{app} (less strong foam) was observed once wormhole formation had begun (Figure 12). For this reason, only the pressure drop at the outlet, dP_out, was used for comparisons of apparent viscosity. Also, the order in which the foam qualities were tested was noted, and if the later tests showed significantly lower viscosities, it was assumed that the wormhole was pushing the foam generation zone close to the exit of the core, and these later data points were discarded (Figure 12b).

The wormhole issue also meant that there were technical challenges in ensuring the repeatability of the experiments, as the core plugs had to be changed after each test due to the damage. Thus, each test was carried out with a different permeability core. For this reason, there was a small uncertainty in the discussion of the results, whether any changes in behavior are due to the surfactant alone or whether there is any effect (or not) due to the variations in permeability.

Finally, during the running of the core flood, when the surfactant solution exited the core and returned to normal laboratory temperature and pressure at the outlet of the second back-pressure regulator (BPR2), any dissolved calcium hydrogen carbonate in the solution underwent the reverse reaction: $Ca(HCO_3)_2 \leftrightarrow CaCO_3 + H_2O + CO_2$. This resulted in a large amount of scale forming within the back-pressure regulator and the effluent tubing. This needed to be cleaned after each test (by reaction with 2 M HCl solution) to prevent blockages occurring.

Core Flood Tests − Nitrogen Foam − Changing Surfactant Concentration. Core flood tests were carried out at 65 °C for both surfactants with a range of different concentrations in the synthetic seawater. The resulting apparent viscosity curves are shown in Figure 13. As expected, both the magnitude of the apparent viscosity and the transition foam quality become smaller as the surfactant concentration reduces. However, betaine still showed reasonable foaming behavior at the low concentrations close to the CMC.

Comparison of the Nitrogen and CO_2 Foaming Behavior. The comparison between the measured apparent viscosities for nitrogen and CO_2 is shown in Figure 14 for two of the concentrations. It can be seen that the type of gas has a significant effect on the viscosity response curves for the selected surfactants.

https://doi.org/10.1021/acs.iecr.2c01186
Ind. Eng. Chem. Res. 2022, 61, 11977−11987

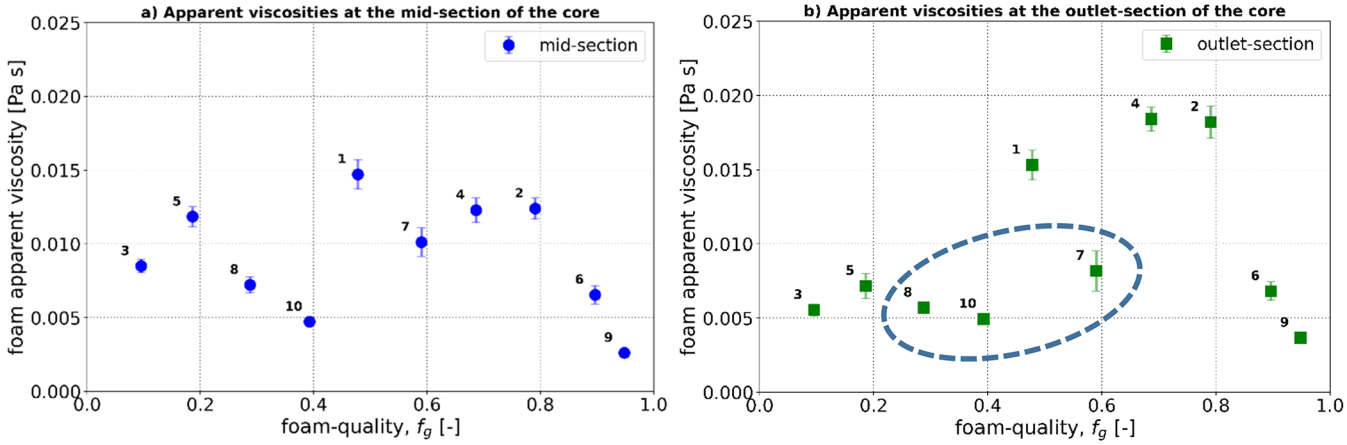

Figure 12. Measured apparent viscosities at (a) the midsection of the core and (b) the outlet of the core, for a preliminary foam-flood test in a 153 mD core. The order in which the tests were carried out is indicated by the labels. The data points circled in (b) were considered to be compromised by the wormhole formation and were thus excluded from any consideration.

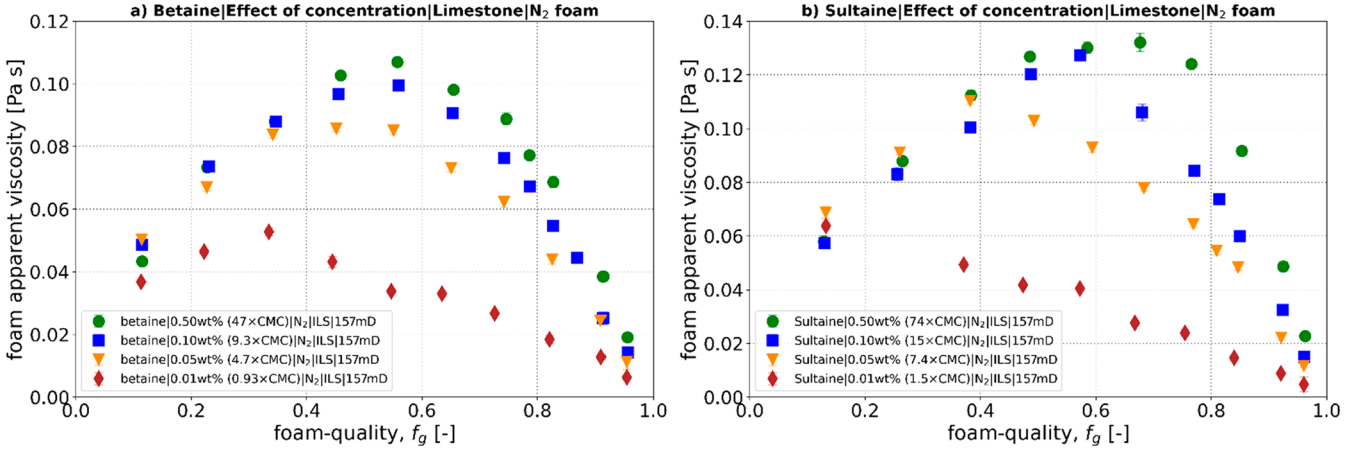

Figure 13. Variation in apparent viscosity for nitrogen foam with changing surfactant concentration for (a) betaine and (b) sultaine.

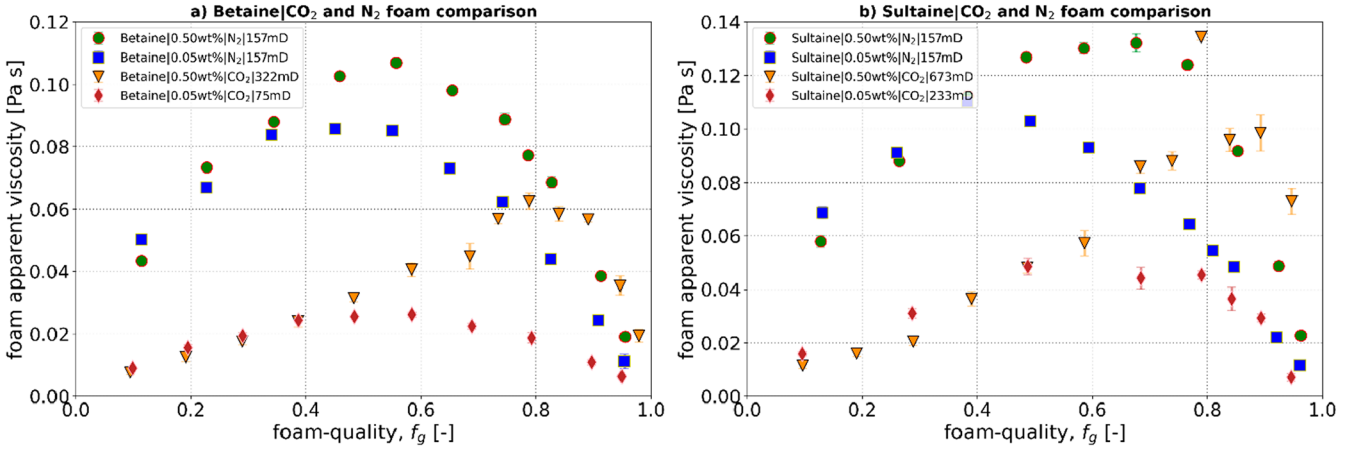

Figure 14. Comparison of apparent viscosity curves for nitrogen and CO_2 foams in Indiana Limestone cores, for (a) betaine and (b) sultaine. The permeability of the limestone core for each case is indicated on the graphs.

Comparing the 0.5 wt % sultaine curves for nitrogen and CO_2, Figure 14b, the maximum apparent viscosity, μ_{max}, is similar in both cases, and the transition foam quality, f_g*, is only slightly higher for the CO_2 (0.8 compared to 0.7 for the nitrogen). This suggests a similar limiting capillary pressure, P_c*, for the two foams.

However, the behavior in the low-foam-quality regime (f_g < 0.8) is significantly different, with much lower viscosities obtained with the CO_2 foam. This is in agreement with the

https://doi.org/10.1021/acs.iecr.2c01186
Ind. Eng. Chem. Res. 2022, 61, 11977−11987

work of Zeng et al.[48] who found that nitrogen gave stronger foams than CO_2.

The shape of the curve for the CO_2 is also unusual, with a more concave shape than expected, particularly when compared to the traditional (convex, shear thinning) curve shape of the nitrogen. Similar behavior, although not as extreme, was observed for the betaine (Figure 14a). It is possible that the lower apparent viscosity in the low-foam-quality regime, which causes this curve shape, is due to the dissolution of some of the CO_2 into the injected water (thus reducing the foam quality and the total flow velocity at the same time), but corrections were already made for the solubility of the CO_2 during the calculation of the gas injection rate. Others have also seen this type of concave curve shape, both with CO_2 in sandstone[37,38,49,50] and in limestone[51,52] and also in tests in capillary tubes.[26,49,51] It is known that gas diffusion through the bubble films is significantly higher for CO_2 than for N_2,[53] which would lead to more rapid foam coarsening. This coarsening, along with the lower pH produced by the CO_2 dissolution, explains the generally weaker foams observed with CO_2.[49] If this weakening effect becomes more significant at lower foam qualities, this would result in the concave curve shape.

Considering the effects of the changing concentration, for the sultaine with nitrogen (Figure 14b), it can be seen that as the concentration drops from 0.5 to 0.05 wt %, the greatest change is the reduction of f_g*. This results in an earlier transition to the high-quality regime and in reduced viscosities at high foam qualities. For the CO_2, because of the concave shape of the curve, the reduction in f_g* resulted in a significantly lower value of the μ_{max}, as compared to the nitrogen. However, the value of f_g* still remained higher for CO_2 than for the nitrogen. This implies a smaller limiting water saturation or higher limiting capillary pressure, which is contrary to conventional surfactants like alpha-olefin sulfonate (AOS).[48] This also indicates that the surfactants selected in this study are more suitable for CO_2 than for nitrogen when foaming behavior is concerned.

A full summary of the values of μ_{max} and f_g* for all the concentrations tested is given in Table 2. It can be seen from this summary that nitrogen is better at maintaining the magnitude of viscosity (higher μ_{max}), but CO_2 is better at maintaining behavior at high foam quality (higher f_g*) as the surfactant concentration falls. This high-foam-quality behavior of CO_2 is useful for any EOR or CCS injection system, where economics and the cost of surfactant indicate a preference for drier foams (lower liquid volume) at low concentrations. In addition, for CCS applications, it is not desirable to have large apparent viscosities, as this may reduce the injectivity of the CO_2 disposal wells. Working at low concentrations (0.05 wt %) and at very high qualities ($f_g \geq 0.95$) therefore has the advantage of being both very economical and producing the minimal increase in apparent viscosity desirable in a CCS injection scenario.

Table 2. Maximum Apparent Viscosity, μ_{app}, and f_g* for Both the Nitrogen and the CO_2 Foams and for a Range of Surfactant Concentrations

		N_2		CO_2	
Surfactant	Concentration	Max. μ_{app} [Pa·s]	f_g*	Max. μ_{app} [Pa·s]	f_g*
Betaine	0.5 wt %	0.107	0.55	0.063	0.8
	0.1 wt %	0.100	0.55	-	-
	0.05 wt %	0.086	0.5	0.026	0.6
	0.01 wt %	0.053	0.35	0.020	0.4
Sultaine	0.5 wt %	0.132	0.7	0.134	0.8
	0.1 wt %	0.127	0.6	-	-
	0.05 wt %	0.110	0.4	0.048	0.6
	0.01 wt %	0.064	0.15	-	-

CONCLUSIONS

A series of experiments have been carried out to determine the stability, adsorption, and foaming behavior of two candidate surfactants for potential foam-assisted EOR or CCS in Indiana Limestone cores.

- The temperature stability tests indicate that both the betaine and the sultaine have good long-term stability (up to 18 weeks) at 60 °C in a synthetic seawater.
- The dynamic retention of the betaine and sultaine onto Indiana Limestone was measured to be 12.6 and 13.0 mg/100 g of rock, respectively. In both cases, however, there was a long tail to the adsorption curve for the surfactant, probably due to multicomponent adsorption behavior, mechanical entrapment, and the heterogeneity of the limestone.
- Sultaine had stronger foaming behavior with CO_2 than the betaine. For both surfactants, reducing the surfactant concentration did not affect the foam viscosity in the low-foam-quality regime but resulted in a reduction of both the transition foam quality and the maximum apparent viscosity. Significantly, the foaming behavior remained reasonable even at concentrations close to the CMC, especially for the betaine.
- The injection of CO_2 under our experimental condition caused significant degradation of the limestone cores, with the generation of wormholes. These wormholes could form quite quickly and were responsible for the short testing lifetime of each core.
- Foam-flood tests were also carried out with nitrogen, which facilitated a longer test lifetime for the limestone core. Both the betaine and the sultaine showed strong foaming behavior with nitrogen and the maximum viscosity again reducing with reducing concentration.
- Comparing the changing concentration tests for nitrogen and CO_2, it was found that the nitrogen gave overall higher values of apparent viscosity, but the CO_2 was better at maintaining behavior at high foam quality. Maintaining foaming behavior at high foam quality is a useful trait for any EOR or CCS system, where the cost of surfactant indicates an economic preference for working with drier foams at lower concentrations.

ASSOCIATED CONTENT

Supporting Information

The Supporting Information is available free of charge at https://pubs.acs.org/doi/10.1021/acs.iecr.2c01186.

The Supporting Information file contains more detailed information on the flow calculations and corrections applied to the CO_2 and nitrogen foam flow tests, as discussed briefly in the Experimental Procedures section. The information has been presented in three sections. **Supporting Information I**: Correcting for CO_2 Solubility and Density Changes at Elevated Pressures

https://doi.org/10.1021/acs.iecr.2c01186
Ind. Eng. Chem. Res. 2022, 61, 11977−11987

and Temperatures. This section provides more in-depth information on the corrections that were made to account for temperature and pressure effects on the CO_2 density and flow rate. **Supporting Information II**: Flow Rates and Corrections for CO_2 Foam Core Floods. The data presented in this section includes the nominal flow rates used to run the experiments, along with the corrected values, which took into account the exact pressure and temperature in the core and laboratory. **Supporting Information III**: Flow Rates and Corrections for Nitrogen Foam Core Floods. The data presented in this section includes the nominal flow rates used to run the experiments, along with the corrected values, which took into account the exact pressure and temperature in the core and laboratory (PDF)

AUTHOR INFORMATION

Corresponding Author

Siân A. Jones − *Delft University of Technology, 2628CN Delft, The Netherlands;* orcid.org/0000-0002-2374-8391; Email: s.a.jones@tudelft.nl

Authors

Siavash Kahrobaei − *Shell Global Solutions International B.V, 1030BN Amsterdam, The Netherlands*

Niels van Wageningen − *Shell Global Solutions International B.V, 1030BN Amsterdam, The Netherlands*

Rouhi Farajzadeh − *Delft University of Technology, 2628CN Delft, The Netherlands; Shell Global Solutions International B.V, 1030BN Amsterdam, The Netherlands;* orcid.org/0000-0003-3497-0526

Complete contact information is available at: https://pubs.acs.org/10.1021/acs.iecr.2c01186

Notes

The authors declare no competing financial interest.

ACKNOWLEDGMENTS

This work was supported by the Shell Global Solutions International B.V.

REFERENCES

(1) Holm, L. W. Carbon Dioxide Solvent Flooding for Increased Oil Recovery. *Trans. AIME* **1959**, *216* (01), 225−231.

(2) Rathmell, J. J.; Stalkup, F. I.; Hassinger, R. C. A Laboratory Investigation of Miscible Displacement by Carbon Dioxide. *Fall meeting of the society of petroleum engineers of AIME* **1971**, SPE-3483-MS.

(3) Martin, D. F.; Taber, J. J. Carbon Dioxide Flooding. *J. Pet. Technol.* **1992**, *44* (04), 396−400.

(4) El-hoshoudy, A. N.; Desouky, S. CO2 Miscible Flooding for Enhanced Oil Recovery. *Carbon Capture, Util. Sequestration* **2018**.

(5) Bui, M.; Adjiman, C. S.; Bardow, A.; Anthony, E. J.; Boston, A.; Brown, S.; Fennell, P. S.; Fuss, S.; Galindo, A.; Hackett, L. A.; Hallett, J. P.; Herzog, H. J.; Jackson, G.; Kemper, J.; Krevor, S.; Maitland, G. C.; Matuszewski, M.; Metcalfe, I. S.; Petit, C.; Puxty, G.; Reimer, J.; Reiner, D. M.; Rubin, E. S.; Scott, S. A.; Shah, N.; Smit, B.; Trusler, J. P. M.; Webley, P.; Wilcox, J.; Mac Dowell, N. Carbon Capture and Storage (CCS): The Way Forward. *Energy Environ. Sci.* **2018**, *11* (5), 1062−1176.

(6) Haszeldine, R. S.; Flude, S.; Johnson, G.; Scott, V. Negative Emissions Technologies and Carbon Capture and Storage to Achieve the Paris Agreement Commitments. *Philos. Trans. R. Soc. A* **2018**, *376* (2119), 20160447.

(7) Metz, B.; Davidson, O.; de Coninck, H.; Loos, M.; Meyer, L. *IPCC Special Report on Carbon Dioxide Capture and Storage*; Cambridge University Press: Cambridge, 2005.

(8) Shelton, J. L.; McIntosh, J. C.; Hunt, A. G.; Beebe, T. L.; Parker, A. D.; Warwick, P. D.; Drake, R. M.; McCray, J. E. Determining CO2 Storage Potential during Miscible CO2 Enhanced Oil Recovery: Noble Gas and Stable Isotope Tracers. *Int. J. Greenh. Gas Control* **2016**, *51*, 239−253.

(9) Ampomah, W.; Balch, R. S.; Grigg, R. B.; McPherson, B.; Will, R. A.; Lee, S.-Y.; Dai, Z.; Pan, F. Co-Optimization of CO2-EOR and Storage Processes in Mature Oil Reservoirs. *Greenh. Gases Sci. Technol.* **2017**, *7* (1), 128−142.

(10) Lashgari, H. R.; Sun, A.; Zhang, T.; Pope, G. A.; Lake, L. W. Evaluation of Carbon Dioxide Storage and Miscible Gas EOR in Shale Oil Reservoirs. *Fuel* **2019**, *241*, 1223−1235.

(11) Farajzadeh, R.; Eftekhari, A. A.; Dafnomilis, G.; Lake, L. W.; Bruining, J. On the Sustainability of CO2 Storage through CO2 − Enhanced Oil Recovery. *Appl. Energy* **2020**, *261*, 114467.

(12) Ringrose, P.; Nazarian, B.; Zadeh, A. M. Keynote: Comparing Benefits of CO2 Storage and CO@EOR from a Climate Mitigation Perspective. *IOR 2021 - 21st Eur. Symp. Improv. Oil Recover.* **2021**, 1−3.

(13) Schramm, L. L., Ed. *Foams: Fundamentals and Applications in the Petroleum Industry*; American Chemical Society, 1994..

(14) Ibrahim, A. F.; Nasr-El-Din, H. A. Stability Improvement of Carbon Dioxide Foam Using Nanoparticles and Viscoelastic Surfactants for Enhanced-Oil-Recovery Applications. *SPE Reserv. Eval. Eng.* **2020**, *23* (02), 414−430.

(15) Jones, S. A.; Laskaris, G.; Vincent-Bonnieu, S.; Farajzadeh, R.; Rossen, W. R. Effect of Surfactant Concentration on Foam: From Coreflood Experiments to Implicit-Texture Foam-Model Parameters. *J. Ind. Eng. Chem.* **2016**, *37*, 268−276.

(16) Kahrobaei, S.; Farajzadeh, R. Insights into Effects of Surfactant Concentration on Foam Behavior in Porous Media. *Energy Fuels* **2019**, *33* (2), 822−829.

(17) Shepherd, M. Carbonate Reservoirs. *Oil Field Production Geology* **2009**, 301−309.

(18) Schlumberger. *Carbonate Reservoirs | Schlumberger*. https://www.slb.com/technical-challenges/carbonates (accessed 2021−09−15).

(19) Hirasaki, G.; Zhang, D. L. Surface Chemistry of Oil Recovery From Fractured, Oil-Wet, Carbonate Formation. *SPE J.* **2004**, *9* (02), 151−162.

(20) Aarra, M. G.; Ormehaug, P. A.; Skauge, A.; Masalmeh, S. K. Experimental Study of CO2- and Methane-Foam Using Carbonate Core Material at Reservoir Conditions. *SPE Middle East Oil Gas Show Conf. MEOS, Proc.* **2011**, *2*, SPE-141614-MS.

(21) Skauge, A.; Solbakken, J.; Ormehaug, P. A.; Aarra, M. G. Foam Generation, Propagation and Stability in Porous Medium. *Transp. Porous Media* **2020**, *131* (1), 5−21.

(22) Kamal, M. S.; Hussein, I. A.; Sultan, A. S. Review on Surfactant Flooding: Phase Behavior, Retention, IFT, and Field Applications. *Energy Fuels* **2017**, *31* (8), 7701−7720.

(23) Gland, N.; Chevallier, E.; Cuenca, A.; Batot, G. New Developement of Cationic Surfactant Formulations for Foam Assisted CO2-EOR in Carbonates Formations. *Soc. Pet. Eng. - Abu Dhabi Int. Pet. Exhib. Conf.* **2018**, SPE-193201-MS DOI: 10.2118/193201-MS.

(24) Jian, G.; Fernandez, C. A.; Puerto, M.; Sarathi, R.; Bonneville, A.; Biswal, S. L. Advances and Challenges in CO2 Foam Technologies for Enhanced Oil Recovery in Carbonate Reservoirs. *J. Pet. Sci. Eng.* **2021**, *202*, 108447.

(25) Kaczerewska, O.; Martins, R.; Figueiredo, J.; Loureiro, S.; Tedim, J. Environmental Behaviour and Ecotoxicity of Cationic Surfactants towards Marine Organisms. *J. Hazard. Mater.* **2020**, *392*, 122299.

(26) Jian, G.; Zhang, L.; Da, C.; Puerto, M.; Johnston, K. P.; Biswal, S. L.; Hirasaki, G. J. Evaluating the Transport Behavior of CO2 Foam

in the Presence of Crude Oil under High-Temperature and High-Salinity Conditions for Carbonate Reservoirs. *Energy Fuels* **2019**, *33* (7), 6038−6047.
(27) Jian, G.; Alcorn, Z.; Zhang, L.; Puerto, M. C.; Soroush, S.; Graue, A.; Biswal, S. L.; Hirasaki, G. J. Evaluation of a Nonionic Surfactant Foam for CO2Mobility Control in a Heterogeneous Carbonate Reservoir. *SPE J.* **2020**, *25* (06), 3481−3493.
(28) Zuta, J.; Fjelde, I. Transport of CO2-Foaming Agents During CO2-Foam Processes in Fractured Chalk Rock. *SPE Reserv. Eval. Eng.* **2010**, *13* (04), 710−719.
(29) Haugen, A.; Fernø, M. A. A.; Graue, A.; Bertin, H. J. J. Experimental Study of Foam Flow in Fractured Oil-Wet Limestone for Enhanced Oil Recovery. *SPE Reserv. Eval. Eng.* **2012**, *15* (02), 218−228.
(30) Eide, Ø.; Fernø, M. A.; Graue, A. Visualization of CO2 EOR by Diffusion in Fractured Chalk. *Proc. - SPE Annu. Technol. Conf. Exhib.* **2014**, *6*, SPE-170920-MS.
(31) Dong, P.; Puerto, M.; Jian, G.; Ma, K.; Mateen, K.; Ren, G.; Bourdarot, G.; Morel, D.; Biswal, S. L.; Hirasaki, G. Exploring Low-IFT Foam EOR in Fractured Carbonates: Success and Particular Challenges of Sub-10-Md Limestone. *SPE J.* **1900**, *25* (02), 867−882.
(32) AlYousef, Z.; Gizzatov, A.; Almajid, M.; Alabdulwahab, A. Rheology, Stability, and Adsorption of an Amphoteric Foaming Agent for CO2 Mobility Control Applications under Reservoir Conditions. *IOR 2021 - 21st Eur. Symp. Improv. Oil Recover.* **2021**, *2021* (1), 1−12.
(33) Kibron. *Ez-Pi +*. https://www.kibron.com/ez-pi-plus-tensiometer#product (accessed 2021−09−15).
(34) Budhathoki, M.; Barnee, S. H. R.; Shiau, B. J.; Harwell, J. H. Improved Oil Recovery by Reducing Surfactant Adsorption with Polyelectrolyte in High Saline Brine. *Colloids Surfaces A Physicochem. Eng. Asp.* **2016**, *498*, 66−73.
(35) Duan, Z.; Sun, R.; Zhu, C.; Chou, I-M. An Improved Model for the Calculation of CO2 Solubility in Aqueous Solutions Containing Na+, K+, Ca2+, Mg2+, Cl−, and SO42−. *Mar. Chem.* **2006**, *98*, 131−139.
(36) Span, R.; Wagner, W. A New Equation of State for Carbon Dioxide Covering the Fluid Region from the Triple-Point Temperature to 1100 K at Pressures up to 800 MPa. *J. Phys. Chem. Ref. Data* **1996**, *25* (6), 1509.
(37) Li, K. *The Effects of Oil on CO2 Foam Flooding under Miscible Conditions*. Master's Thesis, Technical University of Delft, 2016. http://resolver.tudelft.nl/uuid:8b1b2072-4609-4acc-a02e-f925cd6dc205.
(38) Kagoro, R. B. *The Effect of Surfactant Type, Velocity and Permeability on CO 2 Foam under Miscible Conditions*. Master's Thesis, Technical University of Delft, 2017. http://resolver.tudelft.nl/uuid:11985f8c-b27d-424c-a46e-dd947a00adc2.
(39) Mannhardt, K.; Schramm, L. L.; Novosad, J. J. Effect of Rock Type and Brine Composition on Adsorption of Two Foam-Forming Surfactants. *SPE Adv. Technol. Ser.* **1993**, *1* (1), 212−218.
(40) Wang, J.; Han, M.; Fuseni, A. B.; Cao, D. Surfactant Adsorption in Surfactant-Polymer Flooding for Carbonate Reservoirs. *SPE Middle East Oil Gas Show Conf. MEOS, Proc.* **2015**, SPE-172700-MS.
(41) Farajzadeh, R.; Bedrikovetsky, P.; Lotfollahi, M.; Lake, L. W. Simultaneous Sorption and Mechanical Entrapment during Polymer Flow through Porous Media. *Water Resour. Res.* **2016**, *52* (3), 2279−2298.
(42) Ghous, A.; Senden, T. J.; Sok, R. M.; Sheppard, A. P.; Pinczewski, V. W.; Knackstedt, M. A. 3D Characterisation of Microporosity in Carbonate Cores. *SPWLA Middle East Reg. Symp.* **2007**, SPWLA-MERS-2007-E.
(43) Dawson, R.; Lantz, R. B. Inaccessible Pore Volume in Polymer Flooding. *Soc. Pet Eng. J.* **1972**, *12* (5), 448−452.
(44) Brame, S. D.; Mukherjee, B.; Patil, P.; Katiyar, A.; Nguyen, Q. P. The Effect of Rock Microheterogeneity on Steam Foam Rheology. *J. Pet. Sci. Eng.* **2020**, *188*, 106898.
(45) Kapetas, L.; Vincent Bonnieu, S.; Farajzadeh, R.; Eftekhari, A. A.; Shafian, S. R. M.; Bahrim, R. Z. K.; Rossen, W. R. Effect of Permeability on Foam-Model Parameters: An Integrated Approach from Core-Flood Experiments through to Foam Diversion Calculations. *Colloids Surf., A* **2017**, *530*, 172−180.
(46) Regnet, J. B.; David, C.; Robion, P.; Menéndez, B. Microstructures and Physical Properties in Carbonate Rocks: A Comprehensive Review. *Mar. Pet. Geol.* **2019**, *103*, 366−376.
(47) Snippe, J.; Berg, S.; Ganga, K.; Brussee, N.; Gdanski, R. Experimental and Numerical Investigation of Wormholing during CO2 Storage and Water Alternating Gas Injection. *Int. J. Greenh. Gas Control* **2020**, *94*, 102901.
(48) Zeng, Y.; Farajzadeh, R.; Eftekhari, A. A.; Vincent-Bonnieu, S.; Muthuswamy, A.; Rossen, W. R.; Hirasaki, G. J.; Biswal, S. L. Role of Gas Type on Foam Transport in Porous Media. *Langmuir* **2016**, *32* (25), 6239−6245.
(49) Zhou, J.; Srivastava, M.; Hahn, R.; Inouye, A.; Dwarakanath, V. Evaluation of an Amphoteric Surfactant for CO2 Foam Applications: A Comparative Study. *Proc. - SPE Symp. Improv. Oil Recover.* **2020**, SPE-200315-MS.
(50) Føyen, T.; Alcorn, Z. P.; Fernø, M. A.; Barrabino, A.; Holt, T. CO2 Mobility Reduction Using Foam Stabilized by CO2- and Water-Soluble Surfactants. *J. Pet. Sci. Eng.* **2021**, *196*, 107651.
(51) Da, C.; Alzobaidi, S.; Jian, G.; Zhang, L.; Biswal, S. L.; Hirasaki, G. J.; Johnston, K. P. Carbon Dioxide/Water Foams Stabilized with a Zwitterionic Surfactant at Temperatures up to 150 °C in High Salinity Brine. *J. Pet. Sci. Eng.* **2018**, *166* (March), 880−890.
(52) Alsumaiti, A. M.; Hashmet, M. R.; Alameri, W. S.; Anto-Darkwah, E. Laboratory Study of CO2 Foam Flooding in High Temperature, High Salinity Carbonate Reservoirs Using Co-Injection Technique. *Energy Fuels* **2018**, *32* (2), 1416−1422.
(53) Farajzadeh, R.; Vincent-Bonnieu, S.; Bourada Bourada, N. Effect of Gas Permeability and Solubility on Foam. *J. Soft Matter* **2014**, *2014*, 1.

https://doi.org/10.1021/acs.iecr.2c01186
Ind. Eng. Chem. Res. 2022, 61, 11977−11987